A five-link 2D brachiating ape model with life-like zero-energy-cost motions

Mario W. Gomes * Andy L. Ruina

Theoretical and Applied Mechanics, Cornell University, Ithaca, NY 14853, USA

Abstract

We have found periodic life-like brachiating motions of a rigid-body ape model that use no muscle or gravitational energy to move steadily forward. The most complicated of these models has 5 links (a body and two arms each with 2 links) and 7 degrees of freedom in flight. The defining feature of all our periodic solutions is that all collisions are at zero relative velocity. These motions are found using numerical integration and root-finding that is sufficiently precise so as to imply that the solutions found correspond to mathematical solutions with exactly zero energy cost. The only actuation and control in the model is for maintaining contact with and releasing handholds which requires no mechanical work. The similarity of these energy-free simulations to the motions of apes suggests that muscle-use minimization at least partially characterizes the coordination strategies of brachiating apes.

Key words: passive dynamic, brachiation, collisionless, gibbon
PACS: 87.19.St, 45.05.+x, 45.40.-f

1 Introduction

Brachiation is the hand over hand swinging locomotion used by various primates, especially long armed apes. A *continuous contact* brachiating gait is somewhat like upside down walking in that the ape has at least one hand on a handhold at all times. A *ricochetal* gait is something like upside down running in that there is a flight phase between successive handholds,

* Corresponding author
Email addresses: mwg1@cornell.edu (Mario W. Gomes), ruina@cornell.edu (Andy L. Ruina).
URL: http://ruina.tam.cornell.edu/research (Andy L. Ruina).

One approach to understanding animal motions is through kinematics, noting how the body parts' positions, velocities, and accelerations vary in time. Thus, in making an ape model, one might control these angles either with real-time control or matching the joint angles and angular rates at particular points in the motion. In contrast to these approaches, we pursue the hypothesis that apes coordinate their motion in a manner that minimizes their muscular work (Alexander, 2001),(Borelli, 1743, Proposition 166); our model makes no explicit *a priori* attempt to control the kinematics.

The models here are similar to the passive-dynamic models of human walking pioneered by McGeer (1990). McGeer and his successors have designed stable, energy efficient robotic walkers which consist, basically, of sticks connected by hinges, with no control. These walking machines have surprisingly life-like motions while using only small amounts of gravitational energy to walk downhill (Collins et al., 2001). The natural appearance of these passive-dynamic models' motions suggest that a large part of the human walking control strategy is governed by muscle-use minimization. These passive-dynamic walkers can only walk at non-vanishing speeds by using gravitational energy to make up for energy lost at the collision of the foot with the ground. However, here we take the energy minimizations approach to the extreme and seek locomotion with zero energy cost. For the brachiation models presented here, the passive motions use no muscular work or gravitational potential energy.

2 Previous Brachiation Work

The comparison between ape brachiation and the swing of a pendulum goes back to at least to Tuttle (1968). Fleagle (1974)'s film-based kinematics studies led him to postulate that siamangs pump energy into their pendular motions by lifting their legs at the bottom of the motion (much like a child on a swing). Preuschoft and Demes (1984) found that a rigid-object (as opposed to point mass) pendulum well-mimics the motions of relatively long armed-apes in slow continuous-contact brachiation. They mention, but forgo a detailed dynamical analysis of, the appropriateness of a point-mass model for the ricochetal gait. Swartz (1989) used more realistic mass and geometry parameters to evaluate the speed of, and grasping forces used for, a continuous contact gait.

Bertram et al. (1999) thoroughly studied a point-mass collision-free model of both continuous contact and ricochetal brachiation and showed various qualitative agreements with gibbon brachiation kinematics and force data. They concluded that collision avoidance might be a major determinant of brachiation strategies (This model is discussed in the point-mass-model section below). On the other hand, Usherwood and Bertram (2003) noted that gibbons actually overshoot their minimal trajectories slightly, thus apparently inten-

tionally having some small collisional losses. They conjectured that gibbons slightly overshoot the ideal collisionless path because the consequences of undershooting (falling) are prohibitively negative. Usherwood and Bertram also proposed, but did not investigate, a model identical to the "rigid body with massless arm model", in this paper, to help qualitatively explain why a gibbon's body is not in line with its supporting arm for the whole swing phase of a ricochetal gait.

Research on the control of under-actuated systems (systems with fewer actuators than degrees of freedom) has used brachiation as a test-bed to check the efficacy of various control algorithms. Fukuda et al. (1991) have designed, simulated, and built a two degree of freedom brachiating robot with a single actuator between the two links. The robot's adaptive controller allows it to swing up from the static stable equilibrium position and then brachiate on a horizontal ladder with irregularly spaced handholds. Yamafuji et al. (1992) have also designed and built a two-link brachiator controlled by a single actuator at the central link. They use a proportional-derivative controller to implement a prescribed reference trajectory for the two links. Spong (1994) developed a controller for "Acrobot" (a conceptually similar two dimensional, two degrees-of-freedom system with a single actuator in between the links) that could swing up from the stable equilibrium position to an inverted position and balance there. Nishimura and Funaki (1996, 1998) designed, simulated, and built a serial three-link under-actuated brachiating robot with two motors, capable of brachiating under a horizontal support. Odagaki et al. (1997) developed two controllers for an identical serial three-link model. Saito and Fukuda (1997) have designed and built a "realistic" three dimensional robot based closely on the body proportions of a siamang with 12 degrees of freedom and 14 actuators. This robot can swing up and brachiate continuously around and underneath a circular horizontal ladder of handholds. Kajima et al. (2003) have designed and built "Gorilla Robot II" a 19 link robot with 20 actuators that has successfully brachiated using two distinct continuous contact gaits (over-hand and side-hand). Most of the work in robotic brachiation is exclusively concerned with the continuous contact gait. However, Nakanishi and Fukuda have developed a control algorithm for their two-link brachiator allowing their simulation to execute a "leaping maneuver", *e.g.* a single step of ricochetal brachiation (Nakanishi et al., 2000).

There is a slight disconnect between the simple single-link passive swinging models, *e.g.* (Bertram et al., 1999), and these latter actuated multi-degree-of-freedom models, *e.g.* (Saito and Fukuda, 1997): the former models emphasize basic theory, the latter focus on the implementations of control concepts on more complex systems. The work presented here is an attempt to partially bridge that gap. The work was originally motivated by an informal wager with Fukuda *et al.* (private communication at ICRA 97), that their 2-link robot could have energy-free motions. The approach used here is similar in

spirit to Bertram et al. (1999) but with more degrees of freedom.

3 Modeling Approach

We approach the minimum-muscle-work hypothesis by looking for solutions with exactly zero energy cost; the solutions we seek do not demand any joint torque at any time. Because all known candidate muscle-use cost estimates are minimized by zero muscle use, we need not concern ourselves with the form of the objective (cost, energy-use) functional that we minimize. That is, all Hill-type or Huxley-type muscle laws have zero metabolic cost with zero muscle tension. Note again that the solution search here is more stringent than that for downhill passive dynamic walking which has collisional losses; the motions we seek here not only do not use muscle work but do not use up gravitational potential energy either.

All of the models here use one or more perfectly rigid bodies, motion restricted to two dimensions, frictionless hinges, no air resistance, no springs, handholds available everywhere on the "ceiling", and plastic collisions between hand and handhold. Most of these modeling assumptions have been used either implicitly or explicitly in earlier analyses of brachiation.

The plastic collision assumption requires some clarification. When the ape's hand comes into contact with a handhold it grabs on and the interaction is modeled as a *perfectly plastic* collision (coefficient of restitution, $e = 0$). Linear and angular momentum conservation generally demand that mechanical energy be lost in plastic collisions; where the energy goes depends on detailed non-rigid-body mechanics that do not effect the post-collisional rigid-body motions *e.g.* (Chatterjee and Ruina, Dec 1998). However, if the colliding points on two objects have the same velocity when they make plastic contact, then no energy is lost in that "collision" even though it is a plastic or sticking collision. Two things can make contact with zero approach velocity if their approach velocity tends to zero as contact becomes imminent (*e.g.* see Fig. 11). Because our models have no joint or air friction and no negative muscle work, plastic collisions are the only possible way for the system to lose energy and the solutions we seek don't even have that loss.

The holding and release of the handholds is, in principle, energy-free since the act of holding and releasing the handhold does not change the system's energy. The hands of gibbons and other long-armed apes are particularly suited to this task and almost resemble hooks. Although, for actual gibbons, holding on to a handhold surely has some metabolic cost, but we neglect this cost. The energy-free motions we find, although energetically "passive", are not strictly passive because a control action is needed for initiating and releasing the handholds.

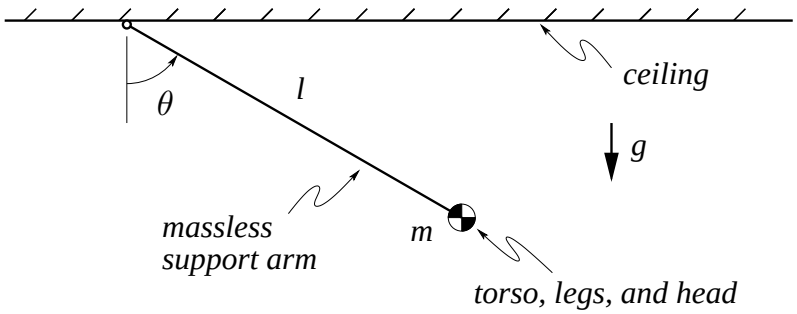

Fig. 1. Point-mass model of a gibbon, from Bertram et al. (1999). This model is capable of collisionless continuous-contact and ricochetal motions (Fig. 2). The torso, legs, and head of the gibbon are all concentrated into a single point mass located at the end of the supporting arm. The arms, being a low proportion of the overall body weight, are treated as massless.

Furthermore, for the first two models below, massless arms swing into place with an energy-free control (non-passive) action.

4 Point-Mass Model

The point-mass-model (Fig. 1) from Bertram et al. (1999) is capable of collisionless continuous-contact and collisionless ricochetal gaits (Bertram et al., 1999). The mass swings from a massless arm which grabs and releases from a ceiling. Collisionless solutions to the model equations can be found by pasting together a concave-up circular arc from the simple pendulum and a concave-down parabolic free-flight (Fig. 2). This model has many energy-cost-free motions. One way of parameterizing these solutions is in terms of the initial condition ($\dot{\theta}(0)$) at the straight down vertical starting position $\theta(0) = 0$.

First consider continuous contact gaits. For any initial $\dot{\theta}(0) < 2\sqrt{g/l}$ the pendulum motion will come to a stop at some height at which point a new pendulum arc with a new handhold can be started. This new arc will obtain the same $\dot{\theta}(0)$ at the bottom ($\theta = 0$) of the next arc thus making up one "step" of a continuous contact gait.

For ricochetal motions, there is a family of solutions for each $\dot{\theta}(0)$ that can be parameterized by the release angle, θ_{rel}, assuming there is enough energy to attain that angle (*e.g.* $0 < \theta_{rel} < \arccos(1 - l\dot{\theta}(0)^2/2g)$).

In the more complex models below, we will similarly parameterize candidate solutions by the state of the system in a symmetry position and, for ricochetal motions, also by a hand-release condition.

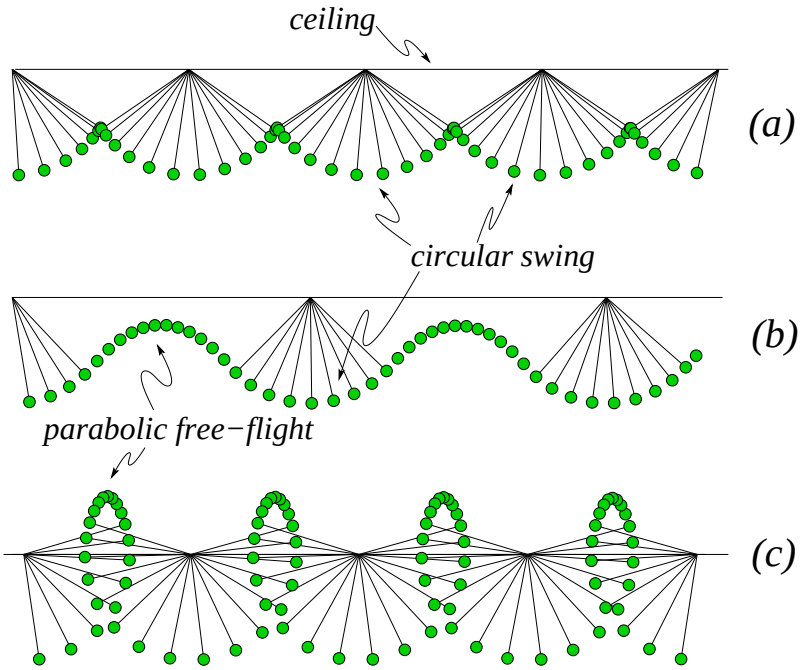

Fig. 2. Solutions of the point-mass model of Fig. 1. Pasting circular swing and parabolic free-flight solutions together will obtain collisionless motions. Solutions (a) and (b) are from Bertram et al. (1999). Figure (c) shows a ricochetal solution for this model which is descriptive of some motions seen in actual gibbon brachiation. Note that $\theta_{rel} > \pi/2$ for motions with a backwards flight phase.

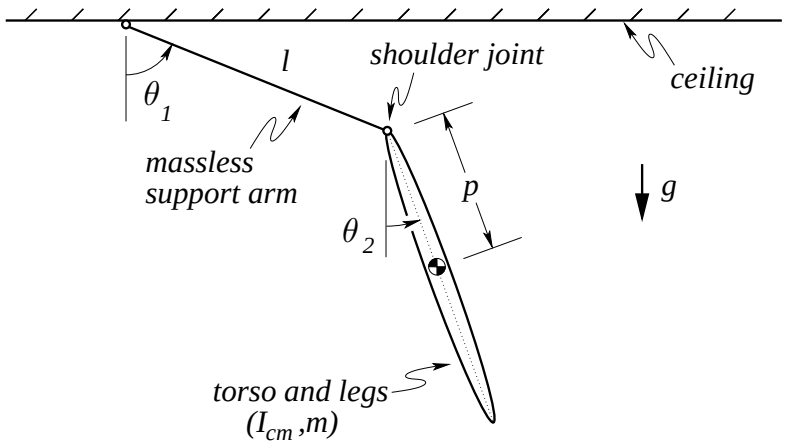

Fig. 3. The single rigid-body model extension of the point-mass model: a rigid body suspended from a massless arm. A right circular cylinder was used to model the single rigid-body which represents the gibbon's combined torso and legs. Parameters are chosen from Preuschoft and Demes (1984) (see appendix B).

5 Rigid-Body Model

We proceed with a sequence of successively more complex models. First we replace the point mass (above) with a rigid body (Fig. 3). The model consists

of a single rigid body (torso, legs, and swing arm) with a non-zero value for its moment of inertia about its center of mass. The mass and geometry parameters used for this model are listed in the caption for Fig. 3 and are taken from Preuschoft and Demes (1984) and discussed in appendix B. In the swing phase a frictionless hinge at one end of the rigid body (the shoulder), connects to the massless rigid arm. In the flight phase, we still use a massless controlled arm. The hand end of the arm grabs the ceiling when it makes contact and lets go when one or another grab/release criteria is met.

For continuous contact motions, the massless arms provide a constraint at all times; one circular shoulder arc connects to the next. For ricochetal motions, the arm constraint is released at $\theta_1(t) = \theta_{rel}$ at the start of flight and reinstated when the distance from the shoulder to the ceiling (in the direction normal to the shoulder velocity) is again equal to the arm length.

Because we have never found asymmetric periodic-collisionless-solutions (for any locomotion model) we only seek solutions that are symmetric about the mid-swing configuration. Thus, we define our initial configuration (at $t = 0$) to have all the links hanging vertical (either straight down or up, as explained further in appendix C.1). Candidate solutions are parameterized by $\dot{\theta}_1$ and $\dot{\theta}_2$ at the assumed symmetric initial condition (θ_{rel} is also part of the parameterization for ricochetal gaits).

We want those values of $\dot{\theta}_1(0)$ and $\dot{\theta}_2(0)$ which result in a collisionless periodic motion. Taking an initial guess at those two values and integrating forward in time, we cease integration when $\dot{\theta}_1 = 0$ (when the support arm is instantaneously at rest). If, at this moment, the orientation of the body is vertical (*i.e.* $\theta_2 = 0$), then the two initial angular velocities are the ones that we desire. This fragment of motion is part of a periodic and collisionless motion because the equations of motion are time-reversible. The motion is periodic since if we begin with those two special values of angular velocity and integrate backwards in time (running time backwards necessarily reverses the signs of the angular velocity), we will obtain the reflected end state when $\dot{\theta}_1 = 0$. Combining the original and reflected pieces gives a complete swing. Since our complete swing begins and ends with $\dot{\theta}_1 = 0$, this periodic motion is also collisionless because the time-reversal of the release action (the collision) involves no velocity discontinuities (*i.e.* since releasing a handhold has no collision, reversing that motion in time results in a collisionless grabbing onto a handhold).

Unlike the situation for the point-mass model, finding these solutions, if they exist, can be a slight challenge. A counting argument suggests the the plausibility of finding solutions. We assume that the mass and geometry properties are given and fixed. To find zero-cost periodic continuous-contact solutions we have two parameters to vary ($\dot{\theta}_1(0)$, $\dot{\theta}_2(0)$) and only one condition to meet ($\theta_2 = 0$ when $\dot{\theta}_1 = 0$), so we expect to find (and do find) a one parameter

family of solutions ($2 - 1 = 1$) (see Table 9). That is, for each $\dot{\theta}_1(0)$ that is not too large we can find a $\dot{\theta}_2(0)$ so that $\theta_2 = 0$ when $\dot{\theta}_1$ reaches zero. Numerical integration of the governing differential equations with the state evaluated when $\dot{\theta}_1 = 0$ gives us the function whose roots we seek (*i.e.* we solve $\theta_2(\text{when } \dot{\theta}_1 = 0) = F(\dot{\theta}_1(0), \dot{\theta}_2(0)) = 0$ where F is evaluated using numerical integration). Appendix A describes the details of the numerical methods. There are many families of solutions having various numbers of swings before the check for $\dot{\theta}_1 = 0$. A simple solution is shown in Fig. 4a.

For ricochetal solutions, we parameterize candidate solutions by $\dot{\theta}_1(0)$, $\dot{\theta}_2(0)$, and θ_{rel}. Using some initial conditions, we integrate forward in time, first using the double-pendulum equations of motion and then, following release, the free-flight equations. When the shoulder reaches a relative maximum in height ($\dot{y}_{shoulder} = 0$) we then seek a symmetric solution (with $\theta_2 = 0$). Since we can vary three initial conditions and are trying to satisfy one condition, we expect to find a two-parameter family of solutions. And, again, it turns out that there are many branches of solutions, some incredibly complex. Two of the collisionless ricochetal motions found are shown in Fig. 4(b,c). Of the many collision-free motions the simpler ones (fewer back and forth swings between handholds, no over-the-top swings, no mid-flight flips) appear to be more gibbon-like when animated.

6 Two-Link Model

The two-link-model consists of two rigid bodies hinged together with a pin joint, a crude approximation of the two arms of a gibbon. The torso, head, and legs are modeled as a heavy point mass located at the hinge between the two arms. Adding a point mass at the hinge is dynamically identical to a modification of the mass distributions of the two links. This model accurately represents the two-link robotic brachiator of Fukuda et al. (1991) after the removal of all their motor torques at the central hinge.

A counting argument for the continuous-contact gaits(see appendix C.2) now predicts only isolated initial conditions leading to periodic zero-collision solutions for a given set of physical parameters. Our numerical searches find many such isolated solutions with varying complexity; we suspect there are an infinite number of these solutions because of the chaotic nature of a double pendulum.

A gibbon-like continuous contact motion is depicted in Fig. 6, and begins with both hands on the ceiling and the whole system motionless. Another gibbon-like continuous-contact motion is depicted in Fig. 7. A somewhat wild non-gibbon-like solution is shown in Fig. 8.

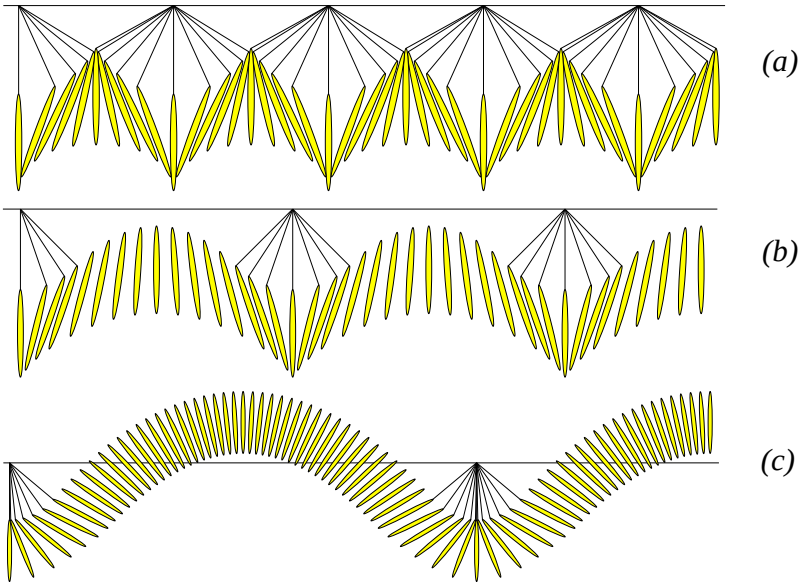

Fig. 4. (a)A continuous-contact motion of the rigid body model. (b)A ricochetal motion of the single rigid body model with a massless arm. Note that the body leads with its feet when approaching the next handhold. (c) Another ricochetal motion. Note that the body leads with its head when approaching the next handhold. The images in (a) are equally spaced in time. The images in (b) and (c) use different time spacings for the swing phase and flight phase so the symmetry, catch, and release positions would be clear. The initial conditions used are: a) θ_1=θ_2=0, $\dot{\theta}_1$ = 9 s^{-1}, $\dot{\theta}_2$ = -8.94693865402 s^{-1}. b) θ_1=θ_2=0, $\dot{\theta}_1$ = 12 s^{-1}, $\dot{\theta}_2$ = -9.993972628 s^{-1}. This motion releases it's hold on the ceiling when $\theta_1 = \pi/4$. c) The initial conditions for (c) are: θ_1=θ_2 = 0, $\dot{\theta}_1$ = 1/10 s^{-1}, $\dot{\theta}_2$ = 17.45530093 s^{-1}. This motion releases the ceiling when $\theta_1 = 5\pi/18$. The large number of digits given is to indicate the accuracy of the numerics and so that the results can be checked.

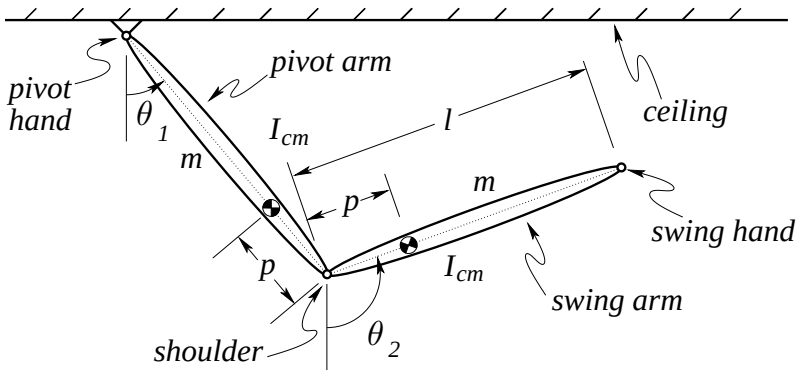

Fig. 5. This is a depiction of the two-link model of a brachiator. The parameters for this model are given in appendix B. Note that the two links have identical parameters as measured from the central hinge at the "shoulder". The torso has been shrunk to a point mass, placed at the central hinge between the two arms, and divided evenly between the two arms for the purpose of calculating the arm's parameters, hence the location of the center of mass is close to the shoulder ($p/l \approx 0.1$).

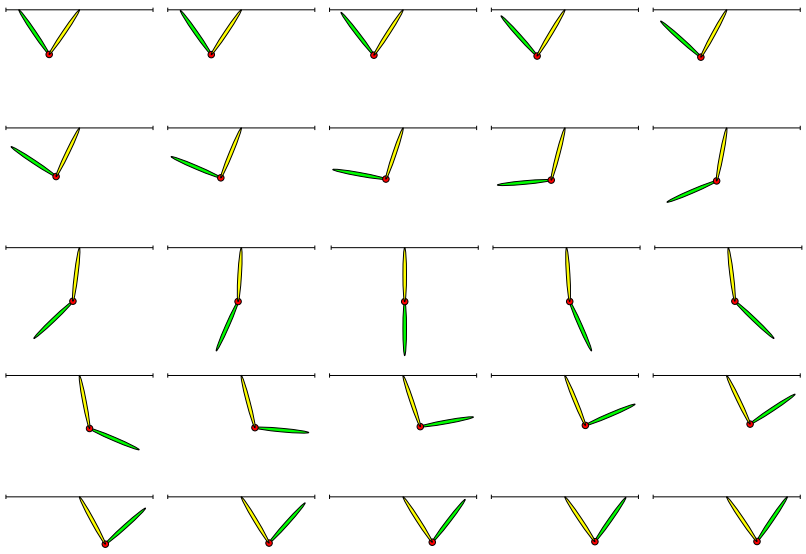

Fig. 6. A gibbon-like continuous contact motion of the two-link model. The initial conditions are: $\theta_1 = 0$, $\theta_2 = 0$, $\dot{\theta}_1 = 1.5505189108055\text{s}^{-1}$, $\dot{\theta}_2 = 11.733043896405\text{s}^{-1}$

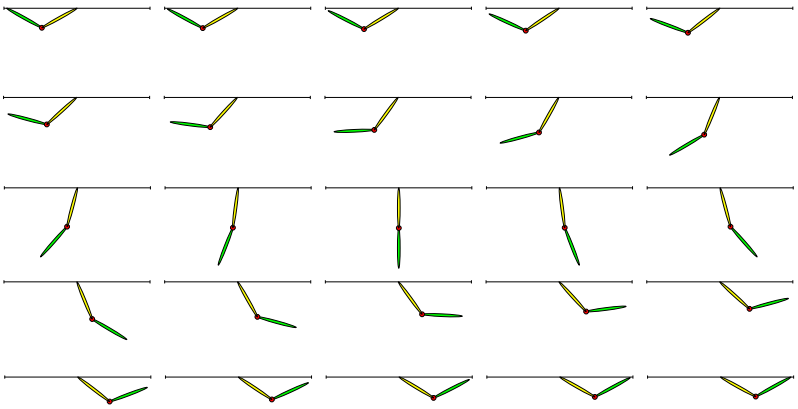

Fig. 7. Another gibbon-like continuous contact motion for the same two-link model. This motion's initial conditions are: θ_1=0, θ_2=0, $\dot{\theta}_1 = 3.560582315550\text{s}^{-1}$, $\dot{\theta}_2 = 10.19595757383\text{s}^{-1}$

For ricochetal gaits with a fixed release angle we also expect only isolated solutions, and many of them. If we allow the release angle to be adjusted we expect many single parameter families of solutions (see 9), only the simplest of which resemble gibbon-like brachiation.

7 Three-Link Model

In the previous model the ape body (torso) was represented by a point mass at the shoulder, here it is extended into a third finite link. This three-link model again has two identical arms (see appendix B for parameters).

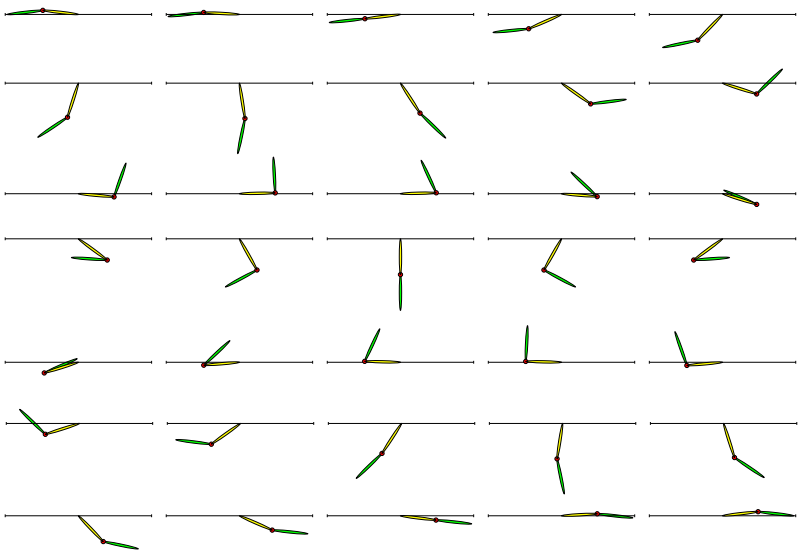

Fig. 8. A more complicated continuous contact motion. Initial conditions are: θ_1=0, θ_2=0, $\dot{\theta}_1 = -6.533304299333\text{s}^{-1}$, $\dot{\theta}_2 = 15.24050128207\text{s}^{-1}$

By symmetry and counting arguments similar to those for the previous models we expect isolated continuous contact solutions and a continuous family of ricochetal solutions parameterized by the release angle θ_{rel} of the swing arm (see 9).

For this more complex model, it is somewhat more difficult to find the desired energy-free motions (root finding procedures fail or lead to odd solutions). So we started with a solution to the two-link model, replacing the point mass with a rigid body with center of mass at the shoulder (which does not change the dynamics at all). Then we repeatedly sought and found solutions with the torso center of mass moved progressively farther from the shoulder (Borzova and Hurmuzlu, 2004) (see appendix A for more details). We then slowly moved the connection hinge away from the center of mass, finding periodic zero-energy solutions with each new parameter set.

We also use this model to illustrate the nature of dissipation-free collisions. Fig. 11 shows the hand positions relative to the next handhold. When the hand reaches the ceiling the slopes of both the horizontal and vertical position curves are zero, indicating that the instantaneous velocity of the hand is zero.

Fig.10 shows one ricochetal periodic collisionless motion for this model.

8 Five-Link Model

Our most complex brachiation simulation is a five-link model. The five links are made up of two forearms, two upper arms, and a torso. This is equivalent

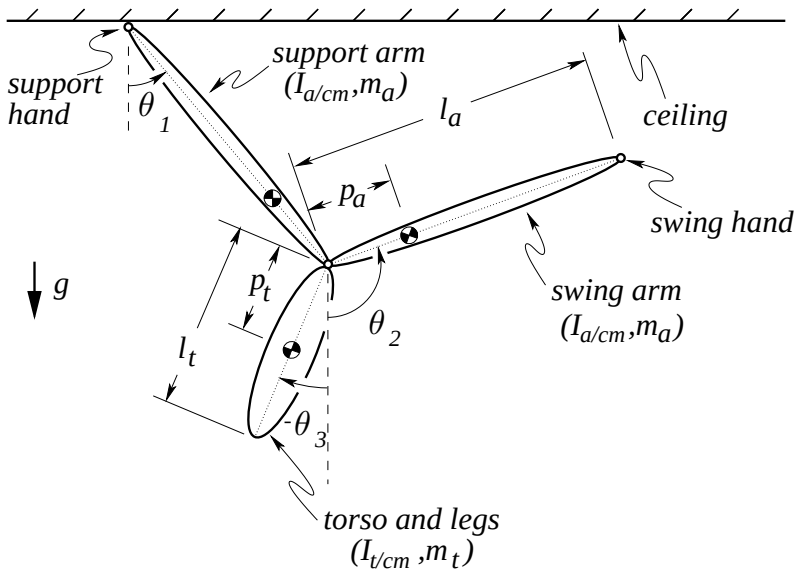

Fig. 9. Three-link model consisting of two arms and a body. Parameter values are given in appendix B.

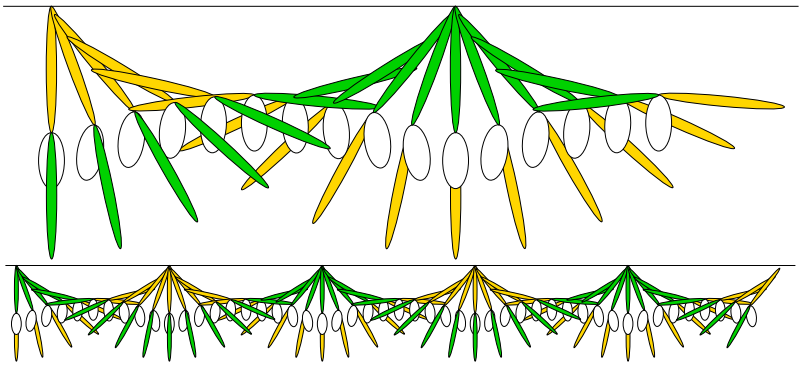

Fig. 10. A Ricochetal Motion for the three-link model: Initial conditions for this motion are: θ_1=0, θ_2=0, θ_3=0, $\dot{\theta}_1 = 9.991543419533\text{s}^{-1}$, $\dot{\theta}_2 = 3.500844111575\text{s}^{-1}$, $\dot{\theta}_3 = -6.919968841782\text{s}^{-1}$. The model releases the ceiling when $\theta_1 = \theta_{rel} = 20°$. This motion is further described by the plot in Figure 11.

to unlocking the elbows of the three-link model.

The parameters used are described in appendix B. The root finding method used to find the motion in Fig. 14 is described in appendix A.

The counting argument that suggests the existence of symmetric motions in the five-link model is similar to the one given for the three link model. Starting at the symmetric hanging position, we have 6 parameters to vary (5 initial angular rates and the angle of the supporting link at release, θ_{rel}). Evaluating the state at a candidate mid-flight condition (when the vertical component of the shoulder velocity is zero) there are 5 symmetry conditions to check ($\alpha = \alpha$, $\beta = \beta$, $\dot{\alpha} = \dot{\alpha}$, $\dot{\beta} = \dot{\beta}$, and $\theta_5 = 0$) (see Fig. 13). Thus we expect to find a one parameter family of solutions ($6 - 5 = 1$) (see Table 9).

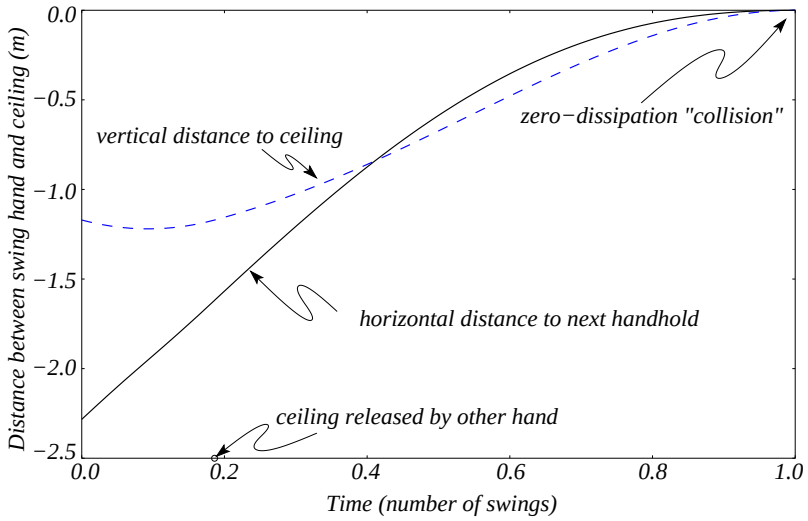

Fig. 11. Vertical and horizontal distance of the swing hand from its impending handhold versus time for the motion in Fig. 10. Note that the slopes of both the horizontal and vertical component are zero, $\dot{x}_{hand}$=$\dot{y}_{hand}$=0 m/s, when the hand collides with the ceiling.

For $\theta_{rel} = 22.3°$ we found two different collisionless periodic solutions, one of which was gibbon-like. See appendix A for a description of the root-finding method. A video of the gibbon-like solution can be seen at: http://ruina.tam.cornell.edu/research.

9 Discussion

The simple brachiation models discussed in this paper attain forward locomotion at zero energy cost and those motions are reminiscent of actual gibbon brachiation.

We have constructed several counting arguments which suggest the existence of the symmetric motions for which we searched. These counting arguments are not rigorous existence proofs but instead are useful for explaining our results and for predicting results for models that were not tested.

All of the collisionless motions that we showed were symmetric. We searched for symmetric motions which, if found, were guaranteed to be collisionless. For the special case of the two-link model, we proved that all of the collisionless motions must be symmetric (see appendix C.2). However, we do not know if all collisionless motions of all symmetric models are symmeteric.

The passive-dynamic walking models studied by McGeer (1990) and others can have periodic motions which are asymptotically stable. Energy flows into the model through gravity as the model walks down the ramp, and energy is

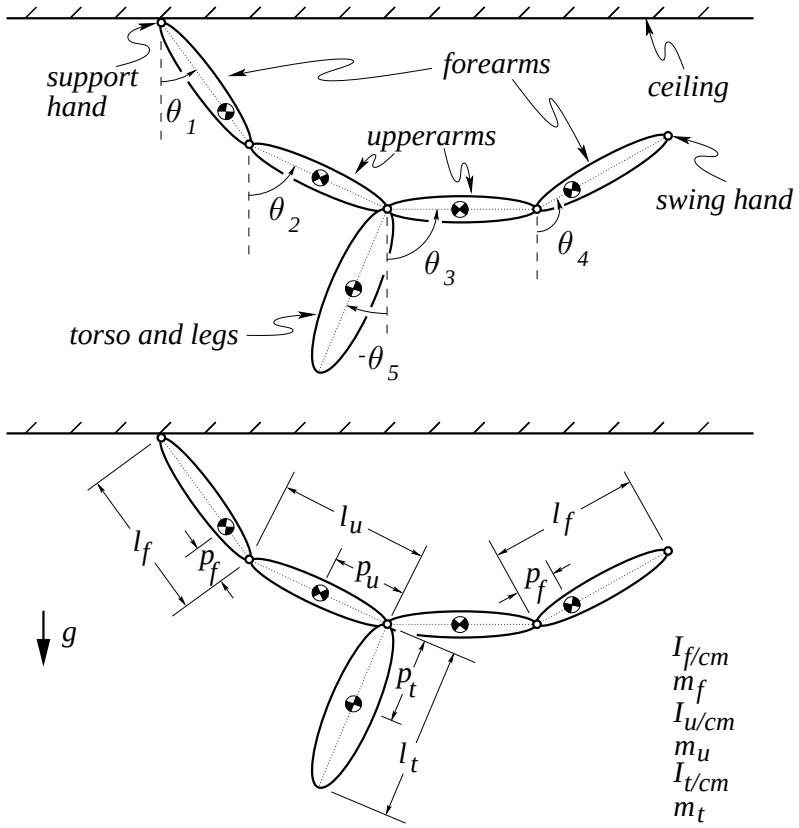

Fig. 12. Five-link model consisting of two forearms, two upperarms, and a body. Parameter values are given in appendix B.

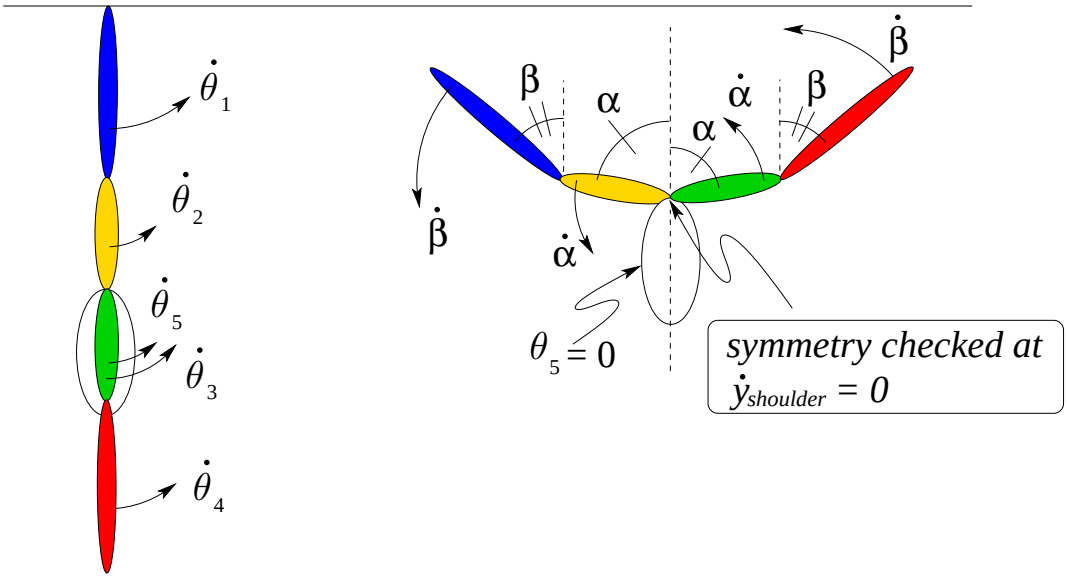

Fig. 13. Criteria for collisionless ricochetal motions for the five link model. The position on the left shows the input state for the map used to find the motion. The position on the right shows the output from the map which would result in a periodic collisionless motion.

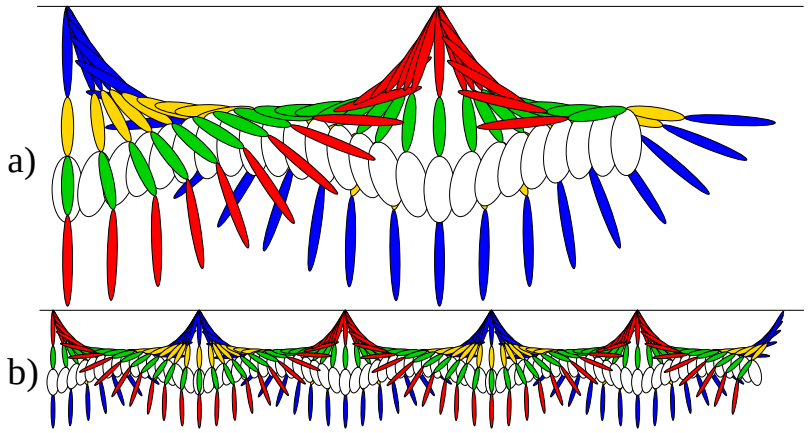

Fig. 14. Snapshots of a periodic collisionless ricochetal motion of the five-link model. Note that the motion begins on the left side of the figures with the models halfway through the swing portion of the gait and ends on the right side of the figures with a) the model halfway through the free flight portion of the ricochetal gait and b) the model just finishing the free flight portion and just grabbing on to the next handhold. The state of the system at mid-swing for this motions is: $\theta_1 = \theta_2 = \theta_3 = \theta_4 = \theta_5 = 0$ $\dot{\theta}_1$= 13.696793227 s^{-1} $\dot{\theta}_2$= -2.4791517485 s^{-1} $\dot{\theta}_3$= 7.9261511913 s^{-1} $\dot{\theta}_4$= -1.7030280005 s^{-1} $\dot{\theta}_5$= -5.6362892519 s^{-1} with $\theta_{rel} = 22.3°$.

lost in collisions at the feet and knees. Just because energy flows in and out of the system does not, in general, imply stability, but for some walking models things work out so that some of the periodic motions are asymptotically stable.

In contrast, the collisionless periodic motions that we have given in this paper are not asymptotically stable. If one perturbs the motion slightly, then the total amount of energy in the system will either increase or decrease. There is no way for any of the models to add energy to the system so perturbations that decrease the system energy can not be corrected and therefore the original periodic motion cannot be regained. If the perturbation increases the systems energy then it may be possible for a plastic collision between the swing hand and the ceiling to decrease the system's total energy, returning the system to the correct amount for the periodic motion. Of course, simply returning the system's energy to the correct amount is not all that is necessary for regaining the periodic motion since there are an infinite number of non-periodic motions with the same total system energy. Thus, the best that one could hope for, in term of stability, for these collisionless periodic motions are that they are one-sided stable, like the hopping motions of Chatterjee et al. (2002). The motions could also be unstable. However, it remains for future work to examine the stability of the collisionless brachiation motions.

A limited mass and length parameter study was done for the two-link brachiation model. Not shown in this paper are solutions found with different parameters than those described in the appendix. Not all of the parameters sets that we tested with this model admitted gibbon-like collisionless motions (see

		Continuous Contact	Ricochetal
Point Mass	free variables:	$\dot{\theta}$ (1)	$\dot{\theta}$, θ_{rel} (2)
	conditions:	n/a (0)	n/a (0)
	solutions:	$1-0 \Rightarrow$ **1 par. family**	$2-0 \Rightarrow$ **2 par. family**
Rigid Body	free variables:	$\dot{\theta}_1$, $\dot{\theta}_2$ (2)	$\dot{\theta}_1$, $\dot{\theta}_2$, θ_{rel} (3)
	section:	(at $\dot{\theta}_1 = 0$)	(at $\dot{y}_{shoulder} = 0$)
	conditions:	$\theta_2 = 0$ (1)	$\theta_2 = 0$ (1)
	solutions:	$2-1 \Rightarrow$ **1 par. family**	$3-1 \Rightarrow$ **2 par. family**
Two Link	free variables:	$\dot{\theta}_1$, $\dot{\theta}_2$ (2)	$\dot{\theta}_1$, $\dot{\theta}_2$, θ_{rel} (3)
	section:	(at $\dot{\theta}_1 = 0$)	(at $\dot{y}_{shoulder} = 0$)
	conditions:	$\dot{\theta}_2 = 0$, $\theta_2 = \pi - \theta_1$ (2)	$\theta_1 = \pi - \theta_2$, $\dot{\theta}_1 = \dot{\theta}_2$ (2)
	solutions:	$2-2=0 \Rightarrow$ **isolated**	$3-2 \Rightarrow$ **1 par. family***
Three Link	free variables:	$\dot{\theta}_1$, $\dot{\theta}_2$, $\dot{\theta}_3$ (3)	$\dot{\theta}_1$, $\dot{\theta}_2$, $\dot{\theta}_3$, θ_{rel} (4)
	section:	(at $\dot{\theta}_1 = 0$)	(at $\dot{y}_{shoulder} = 0$)
	conditions:	$\dot{\theta}_2 = 0$, $\dot{\theta}_3 = 0$, $\theta_2 = \pi - \theta_1$ (3)	$\theta_1 = \pi - \theta_2$, $\dot{\theta}_1 = \dot{\theta}_2$, $\theta_3 = 0$ (2)
	solutions:	$3-3=0 \Rightarrow$ **isolated***	$4-3 \Rightarrow$ **1 par. family**
Five Link	free variables:	$\dot{\theta}_1$, $\dot{\theta}_2$, $\dot{\theta}_3$, $\dot{\theta}_4$, $\dot{\theta}_5$ (5)	$\dot{\theta}_1$, $\dot{\theta}_2$, $\dot{\theta}_3$, $\dot{\theta}_4$, $\dot{\theta}_5$, θ_{rel} (6)
	section:	(at $\theta_5 = 0$)	(at $\dot{y}_{shoulder} = 0$)
	conditions:	$\theta_1 = \pi - \theta_4$, $\theta_2 = \pi - \theta_3$, $\dot{\theta}_1 = \dot{\theta}_4$, $\dot{\theta}_2 = \dot{\theta}_3$, $\dot{y}_{hand} = 0$ (5)	$\theta_1 = \pi - \theta_4$, $\theta_2 = \pi - \theta_3$, $\dot{\theta}_1 = \dot{\theta}_4$, $\dot{\theta}_2 = \dot{\theta}_3$, $\theta_5 = 0$ (5)
	solutions:	$5-5=0 \Rightarrow$ **isolated***	$6-5 \Rightarrow$ **1 par. family**

Table 1
Counting arguments for predicting the existence of symmetric solutions for several brachiation models. We assume symmetric motions for all models. For each model the free variables in the integration for a given set of mass and length parameters are listed with the total number of them in parentheses. the "section" is the state at which symmetry is checked. The "conditions" are the restrictions, at the section, that determine symmetry. The predicted dimension of the solution space is determined by subtracting the number of conditions from the number of free variables. The free parameters are given with $\theta_i = 0$. The solutions families that are marked ("*") were not simulated and the counting argument is given as a prediction. Note that once the model has dispensed with the massless arm (top two cases), a pattern can be seen with isolated continuous contact solutions and single parameter families of ricochetal solutions.

Gomes (2005)). It would be more comforting to have a model which exhibits the same behavior for a wide range of system parameters. However, given the approximate nature of our model as a gibbon, it is pleasing to find motions similar to brachiation for parameters which can be argued as reasonably close to actual gibbons. For example, Coleman (1998) 3D passive walker walks sta-

bly, but its mass distribution is completely non-anthropomorphic with the center of mass of each leg located down near the feet and laterally away from leg.

In a more general sense, these gibbon models support the following claim.

> *If a motion seems intuitively plausible and is consistent with basic momentum and energy considerations, a solution to the dynamics equations with that motion exists.*

In this research by "motion" we mean a periodic solutions that is somewhat life-like in appearance. This is not a theorem, or even the basis of a candidate theorem. But has been the rule, rather than the exception for a host of passive-dynamic walking and brachiating models, and we expect this observation to hold for fully actuated models as well. The counting arguments buttress the concept; if finding solutions is equivalent to solving n equations for n or less conditions it is reasonable to hope to find solutions. But there are, of course exceptions. Not all mass and geometry parameters admit life-like collisionless motions.

The claims in this paper are two-fold, mathematical and relevant for explaining animal motion.

1) Our mathematical claim is that the governing equations of rigid-body mechanics have gibbon-like solutions with (mathematically) zero energy cost. One may distrust a numerical answer to an essentially mathematical question. So in our numerics we have taken care with convergence, event detection, and root finding and thus we believe that our solutions correspond to proper mathematical solutions. We have presented parameters and initial conditions with many digits so others can check this claim with their own numerics.

2) The motions found are also reminiscent of the motions of real gibbons. The zero-energy-cost solutions that solve the governing equations for the models, particularly the solutions of the 5-link model, are somehow beautiful (as seen in the video at `http://ruina.tam.cornell.edu/research`). Thus some version or other of the following class of vague hypotheses is supported: *animals make use of natural dynamics, animals minimize muscle use, or animals minimize muscular work.*

10 Acknowledgments

This work was partially funded by an NSF biomechanics grant and NSF IGERT program. We thank John Bertram for his conversations about gibbon

brachiation as well as for video of actual gibbon brachiation used to make the comparisons with the dynamic models. We thank Richard Rand for explanations of nonlinear normal modes. We also appreciate the insightful comments on the models from Dave Cabrera, Manoj Srinivasan, and Mike Coleman.

References

Alexander, R. M., Aug. 2001. Design by numbers. Nature 412, 591.

Bertram, J. E. A., Ruina, A., Cannon, C. E., Chang, Y. H., Coleman, M. J., 1999. A point-mass model of gibbon locomotion. Journal of Experimental Biology 202, 2609–2617.

Borelli, G. A., 1743. On the movement of animals. Springer Verlag.

Borzova, E., Hurmuzlu, Y., 2004. Passively walking five-link robot. Automatica 40, 621–629.

Chatterjee, A., Pratap, R., Reddy, C., Ruina, A., July 2002. Persistent passive hopping and juggling is possible even with plastic collisions. The International Journal of Robotics Research 21 (7), 621–634.

Chatterjee, A., Ruina, A., Dec 1998. Two interpretations of rigidity in rigid body collisions. Journal of Applied Mechanics 65 (4), 894–900.

Coleman, M. J., Februrary 1998. A stability study of a three-dimensional passive-dynamic model of human gait. Ph.D. thesis, Cornell University, Department of Theoretical and Applied Mechanics.

Collins, S., Wisse, M., Ruina, A., July 2001. A 3-d passive-dynamic walking robot with 2 legs and knees. International Journal of Robotics Research 20 (7), 607–615.

Erikson, G., 1962. Brachiation in new world monkeys and in anthropoid apes. Zoological Society of London ? (10), 135–164.

Fleagle, J., 1974. Dynamics of a brachiating siamang. Nature 248, 259–260.

Fukuda, T., Hosokai, H., Arai, F., Nov. 1991. A study on the brachiation type of mobile robot: Heuristic creation of driving input and control using cmac. IEEE/RSJ International Workship on Intelligent Robots and Systems, IROS '91 ?, 478–483.

Gomes, M. W., January 2005. Collisionless rigid body locomotion models and physically based homotopy methods for finding periodic motions in high degree of freedom models. Ph.D. thesis, Cornell University, Department of Theoretical and Applied Mechanics.

Henon, M., 1982. On the numerical computation of poincare maps. Physica 5D ?, 412–414.

Kajima, H., Hasegawa, Y., Fukuda, T., 2003. Learning algorithm for a brachiating robot. Applied Bionics and Biomechanics 1 (1), 57–66.

McGeer, T., 1990. Passive dynamic walking. The International Journal of Robotics Research 9 (2), 62–82.

Nakanishi, J., Fukuda, T., Koditschek, D. E., 2000. A brachiating robot controller. IEEE Transactions on Robotics and Automation 16 (2), 109–123.

Napier, J. R., Napier, P. H., 1967. A Handbook of Living Primates. Academic Press Inc. (London) Ltd.

Nishimura, H., Funaki, K., Dec. 1996. Motion control of brachiation robot by using final-state control for parameter-varying systems. Proceedings of the 35th Conference on Decision and Control, 2474–2475.

Nishimura, H., Funaki, K., 1998. Motion control of three-link brachiation robot by using final-state control with error learning. IEEE/ASME Transactions on Mechatronics 3 (2), 120–128.

Odagaki, H., Moran, A., Hayase, M., July 1997. Analysis of the dynamics and nonlinear control of under-actuated brachiation robots. Proceedings of the 35th SICE Annual Conference ?, 2137–1142.

Preuschoft, H., Demes, B., 1984. Biomechanics of Brachiation. Edinburgh University Press, pp. 96–118.

Saito, F., Fukuda, T., 1997. A First Result of The Brachiator III–A New Brachiation Robot Modeled on a Siamang. MIT Press, Ch. 43, pp. 354–361.

Schultz, A. H., May 1933. Observations on the growth, classification and evolutionary specialization of gibbons and siamangs. Human Biology 5 (2), 212–255.

Schultz, A. H., September 1933. Observations on the growth, classification and evolutionary specialization of gibbons and siamangs (continued). Human Biology 5 (3), 385–428.

Spong, M. W., 1994. Swing up control of the acrobat. Proceedings IEEE International Conference on Robotics and Automation ?, 2356–2361.

Swartz, S. M., 1989. Pendular mechanics and the kinematics and energetics of brachiating locomotion. International Journal of Primatology 10 (5), 387–418.

Tuttle, R. H., 1968. Does the gibbon swing like a pendulum? American Journal of Physical Anthropologists 29, 132.

Usherwood, J. R., Bertram, J. E., 2003. Understanding brachiation: insight from a collisional perspective. The Journal of Experimental Biology 206, 1631–1642.

Yamafuji, K., Fukushima, D., Maekawa, K., 1992. Study of a mobile robot which can shift from one horizontal bar to another using vibratory excitation. JSME International Journal 35, 456–461.

A Numerical Methods

The equations of motion for the three and five link models were too lengthy to generate explicitly. In our implementation, the set of state derivatives were numerically calculated at each step of the integration. The method of assembling

the equations of motion is described in (Gomes, 2005).

We numerically integrated our equations of motion using an explicit, constant step-size, fourth-order, Runge-Kutta integration routine. We used a change-of-variables method, developed by Henon (1982), to find the exact time of events (*e.g.* when the ceiling release angle was reached, when the vertical component of the shoulder's velocity equals zero, or when the angular velocity of one of the links equals zero).

Using the map constructed above, we conduct a search in the initial condition space for roots. This search was done using a Newton-Raphson root-finding algorithm. For this rootfinding method to converge, an initial guess (for the initial conditions) must be sufficiently close to the actual root. For simple models, like the rigid-body model, intuition in making those guesses was sufficient. For the two-link model, we chose to investigate the range of possible solutions, including ones that we would not initially guess were there. To satisfy our desire for thoroughness, we chose a brute force method to search the two-dimensional initial condition space consisting of two variables, an energy and initial phase angle, $\phi = atan2(\dot{\theta}_1, \dot{\theta}_2)$ We limited our search space to lower energies and $0 \leq \phi \leq \pi$. This bounded initial condition space was then gridded and the rootfinding was conducted using each point on the grid. All of the initial conditions listed in the paper reflect convergence tests that estimate the shown number of significant figures.

For the three and five link models, we started our search using roots found for a simpler model. For the three link model, we began with one of the collisionless continuous-contact motions of the two link model. We then allowed it to release the ceiling to find a ricochetal motion. To move from the two link model to the three link model and maintain the desired two-link model motion, we needed to add a degree of freedom in a smooth manner. We did this by changing the point mass located at the shoulder which represents the torso and legs into a rigid body. By attaching this rigid body by a frictionless hinge at its center of mass to the system, we have uncoupled its rotational dynamics from the rest of the system. Then moved the connection point, in a series of steps, from the center of mass to the end of the torso link. Repeated rootfinding during this process allowed us to track the motion to the three-link model. The motion for the five-link model was found by a similar process. Here, instead of adding a link, we broke two of the arm links in half. This was done by slowly unlocking the elbow joints. We assigned an inertia to the amount of bend in the two elbows and then progressively diminished this inertia from an infinite value to zero. At infinite relative-rotation inertia, the model is equivalent to the three-link model. At zero relative-rotation inertia the model is equivalent to the five-link model. The value of this inertia was then lowered to zero resulting in no rotational coupling at the joints. Although, we at first believed that we had successfully tracked the motion, upon closer examination, we

found that the path curved abruptly and our solutions jumped off of the path onto another path that led to the gibbon-like motion shown. We later, more carefully, followed the original path to find that it ends in a non gibbon-like motion of the five-link system, shown in Gomes (2005).

B Parameters

All of the parameters in the models we considered are based on values from the literature with some modifications (Preuschoft and Demes, 1984; Swartz, 1989; Schultz, May 1933; Erikson, 1962; Schultz, September 1933). Those values are, in turn, derived from gibbon cadaver studies and then approximated to be cylinders in order to calculate their masses and moments of inertia. There is some debate in the literature on what parameters to use; for example, Swartz (1989) disagrees with the parameters given by in Preuschoft and Demes (1984) for a single rigid body model in continuous contact brachiation. Fig. B.1 shows a pictogram of the parameters of the gibbon that we used in the simulations.

Since we could find no complete set of mass and geometry parameters for an "average gibbon" in the existing literature on gibbon biomechanics, we mixed much of the existing data (Schultz (May 1933); Swartz (1989); Schultz (September 1933); Napier and Napier (1967); Preuschoft and Demes (1984)) together, made some measurements from Erikson's x-ray images Erikson (1962), and some educated guesses to come up with the numbers given in Figure B.1. For all of the models with a torso modeled as a rigid body, we compressed the legs and feet into a point mass placed at the bottom of the torso link.

B.1 Rigid-Body model parameters

$l = 0.55\text{m}$, $m = 5.07\text{kg}$, $p = 0.30\text{m}$, $g = 9.81\text{m/s}^2$. The body cylinder is 0.60 meters long (l_{bod}) with a diameter of 0.25 meters ($2r_{bod}$) and is attached to the arm with a frictionless hinge on the top circular plate of the cylinder. The cylinder's moment of inertia about its center of mass is calculated as follows: $I_{cm} = \frac{1}{12}m(3r_{bod}^2 + l_{bod}^2) \approx 0.172\text{kg} \cdot \text{m}^2$. Unless indicated, the numbers are exactly those used in the simulation (*i.e.* the moment of inertia is a derived quantity, calculated in the simulation using the exact values of m, r_{bod}, and l_{bod} given above). We don't use Preuschoft and Demes (1984) support arm parameters. Instead, since a gibbon's arms are a small percentage of their total body weight, we assume that the supporting arm is massless.

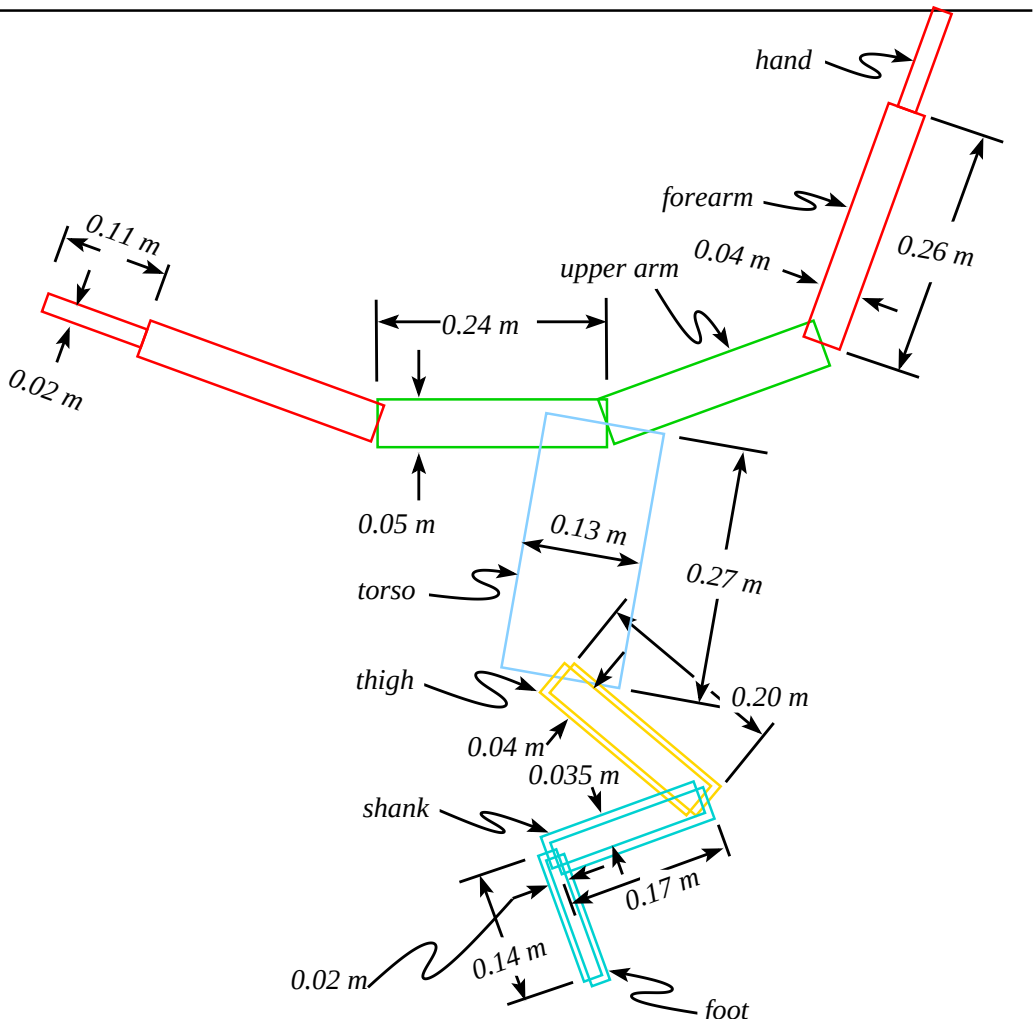

Fig. B.1. Cylindrical Body Segment Gibbon for Visualizing Parameters. The density used for all cylinders was 1000 kg/m^3.

B.2 Two-Link parameters

The parameters for the two link model are easily derived from the model depicted in Fig. B.1. The hand, forearm, and upper arm cylinders are kept in a straight line and glued to each other so that no relative motion between links is possible. The torso, 2 thighs, 2 shanks, and 2 feet cylinders are all compressed upward toward the shoulder into a point mass located at the shoulder pin joint. If the point mass at the shoulder is split in half and half is stuck onto the end of one arm link and the other half stuck to the other arm link then model has the following dimensional parameters: $l = 0.610\ 000\ 000\ 000\ 000$ m, $m = 3.083\ 276\ 839\ 957\ 533$ kg, $p = 6.376\ 870\ 661\ 657\ 008 \times 10^{-2}$ m, $I_{cm} = 5.386\ 568\ 898\ 408\ 416 \times 10^{-2}$ m^{2}kg, $g = 9.810\ 000\ 000\ 000\ 000$ m/s^2. Note that three of the above values (m, p, I_{cm}) are derived quantities, and are calculated based on the exact cylindrical values (given in Fig. B.1) using the

body part	length(m) (exact)	radius(m) (exact)	volume(m^3) (approximate)	mass(kg) (approximate)	$I_{cm}(kg \cdot m^2)$ (approximate)
hand	0.11	0.01	0.3456×10^{-4}	0.03456	0.0357×10^{-3}
forearm	0.26	0.02	3.267×10^{-4}	0.3267	1.873×10^{-3}
upperarm	0.24	0.025	4.712×10^{-4}	0.4712	2.334×10^{-3}
torso	0.27	0.065	35.84×10^{-4}	3.584	25.56×10^{-3}
thigh	0.20	0.02	2.513×10^{-4}	0.2513	0.8629×10^{-3}
2 thighs	0.20	—	—	0.5027	1.726×10^{-3}
shank	0.17	0.0175	1.636×10^{-4}	0.1636	0.4064×10^{-3}
2 shanks	0.17	—	—	0.3271	0.8128×10^{-3}
foot	0.14	0.01	0.456×10^{-4}	0.04398	0.0729×10^{-3}
2 feet	0.14	—	—	0.08796	0.1458×10^{-3}

Table B.1
Approximate model parameter values for each of the cylindrical body segments shown in Figure B.1. Note that for the thighs, shanks, feet, we merge the two cylinders into a single rigid body. $I_{cm} = m/12(3r^2 + l^2)$ is the moment of inertia of the body part about its center of mass. The center of mass is located in the middle of each cylindrical body segment.

parallel axis theorem. The large number of significant figures is given so that one can more easily check our results; since we give our periodic motions with a high degree of accuracy, one needs parameter values with similar accuracy to replicate the simulations. The parameter values are also given as a reference so that the intermediate calculation of the simulation parameters can also be checked.

The arm mass is approximately 0.833 kg and the total mass of the gibbon is approximately 6.17 kg (close to the average total mass of a Hylobate given by Napier and Napier Napier and Napier (1967)). These masses result in an arm to total mass ratio of about 13.5%, which is very close to the 12.5% given by Preushoft and Demes in Preuschoft and Demes (1984).

B.3 Three-Link Model

The lower limbs are more difficult to accurately represent in these models because assumptions must be made as to the posture of the legs and whether to keep the posture fixed while moving. Most gibbons ricochetally brachiate with their legs tucked up underneath their body but use different postures for the continuous contact gait. There are some who believe that the gibbon

raises and lowers their legs to "pump" energy into the movement Fleagle (1974). Active pumping of the lower limbs will have an effect on the dynamics of the system. Thus reducing the legs and torso to a single rigid body appears to be a cruder approximation than reducing each arm to a single rigid body.

For the present work we assume the legs are tucked up under the body and model that assumption by shrinking both thighs, both shanks, and both feet into a point mass on the bottom of the torso. We could have also keep the legs as cylinders and locked the hip joints, knee joints, and ankle joints in the tucked up position but we did not choose that option.

The arm link is constructed from the body parts shown in Figure B.1 by locking the elbow and wrist joints so that the upperarm, forearm, and hand is in a straight line. The body link consists of the torso with the 2 thighs, 2 shanks, and 2 feet compressed to a single point mass and glued to the bottom of the torso cylinder. The center of mass locations are given as distances from the central shoulder hinge. This results in the following dimensional parameters used in the three link model. $p_a = 2.361\ 698\ 113\ 207\ 547\ \times 10^{-1}\mathrm{m}$, $I_{a/cm} = 1.996\ 877\ 403\ 975\ 391\ \times 10^{-2}\mathrm{m}^2\mathrm{kg}$, $l_a = 6.100\ 000\ 000\ 000\ 000\ \times 10^{-1}\mathrm{m}$, $m_a = 8.325\ 220\ 532\ 012\ 952\ \times 10^{-1}\mathrm{kg}$, $p_t = 1.625\ 228\ 997\ 644\ 596\ \times 10^{-1}\mathrm{m}$, $I_{t/cm} = 3.887\ 260\ 478\ 522\ 196\ \times 10^{-2}\mathrm{m}^2\mathrm{kg}$, $l_t = 2.700\ 000\ 000\ 000\ 000\ \times 10^{-1}\mathrm{m}$, $m_t = 4.501\ 509\ 573\ 512\ 475\ \mathrm{kg}$, $g = 9.810\ 000\ 000\ 000\ 000\ \mathrm{m/s}^2$.

B.4 Five-Link Model

The parameters for the five link model are a simple extension of those used in the three link model. In the five link model the arm links both have an "elbow" pin joint between the upperarm and the forearm. The forearm and the hand are still locked together with no relative rotation allowed between those links.

The forearm link is constructed from the body parts shown in Figure B.1 by locking the wrist joint so that the forearm and hand is in a straight line. The body link consists of the torso with the 2 thighs, 2 shanks, and 2 feet compressed to a single point mass and glued to the bottom of the torso cylinder. The center of mass locations for the torso and upperarms are given as distances from the central shoulder hinge along the given rigid body. The center of mass location for the forearm is measured from the elbow joint. $m_f = 3.612\ 831\ 551\ 628\ 263\ \times 10^{-1}\mathrm{kg}$, $l_f = 3.700\ 000\ 000\ 000\ 000\ \times 10^{-1}\mathrm{m}$, $p_f = 1.476\ 956\ 521\ 739\ 130\ \times 10^{-1}\mathrm{m}$, $I_{f/cm} = 2.978\ 536\ 710\ 015\ 953\ \times 10^{-3}\mathrm{m}^2\mathrm{kg}$, $m_u = 4.712\ 388\ 980\ 384\ 690\ \times 10^{-1}\mathrm{kg}$, $l_u = 2.400\ 000\ 000\ 000\ 000\ \times 10^{-1}\mathrm{m}$, $p_u = 1.200\ 000\ 000\ 000\ 000\ \times 10^{-1}\mathrm{m}$, $I_{u/cm} = 2.335\ 577\ 788\ 403\ 162\ \times 10^{-3}\mathrm{m}^2\mathrm{kg}$, $m_t = 4.501\ 509\ 573\ 512\ 475\ \mathrm{kg}$, $l_t = 2.700\ 000\ 000\ 000\ 000\ \times 10^{-1}\mathrm{m}$, $p_t = 1.625\ 228$

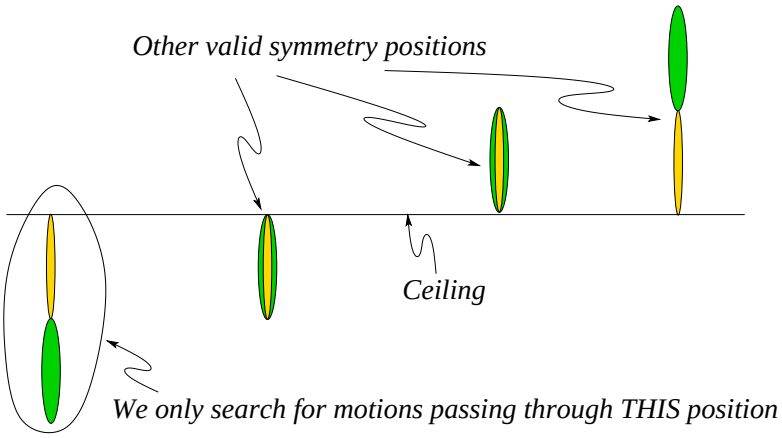

Fig. C.1. Possible central symmetry positions

997 644 596 $\times 10^{-1}$m, $I_{t/cm} = 3.887\ 260\ 478\ 522\ 196\ \times 10^{-2}$m^{2}kg, $g = 9.810\ 000\ 000\ 000\ 000$ m/s^2.

C Two-Link Model Details

C.1 Restrictions on the search space

The collisionless periodic motions of the two-link model we sought require that the "swing hand" have zero velocity at ceiling height. We enforce this criteria by requiring that both links should be at zero angular velocity when the swing hand reaches ceiling height. This is not the only way for the zero velocity criterion to be met. There are two sets of configurations for the system where both links have non-zero angular velocity yet have a "swing hand" that is instantaneously at rest. One set of configurations has $\theta_1 = \theta_2 = \pi/2$ and $\dot{\theta}_1 = -\dot{\theta}_2$. The other set of configurations has $\theta_2 = \theta_1 + \pi$ and $\dot{\theta}_1 = \dot{\theta}_2$. All other configurations require that both $\dot{\theta}_1 = 0$ and $\dot{\theta}_2 = 0$ for the "swing hand" velocity to be equal to zero. We have ignored those solutions which have non-zero angular velocity when the swing hand is at ceiling height.

The symmetry argument given in appendix C.2 shows that all of the motions that we seek must have mirror image symmetries about a vertical line passing through the swing handhold. For the two-link model we have four such candidate positions, depicted in Fig. C.1.

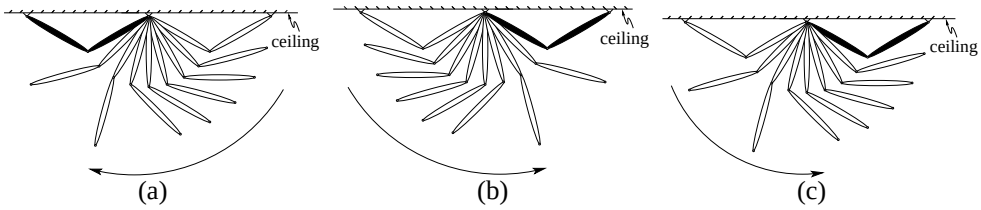

Fig. C.2. (a)Tentative trajectory for system. (b)Trajectory for mirrored initial conditions. (c)The original trajectory under a time reversal. Since (b) and (c) must be identical, the non-symmetric solution shown is not possible.

C.2 Symmetry of solutions

We use proof by contradiction to show that collisionless motions for the two-link model must be symmetric. First we assume that we have a non-symmetric collisionless motion (moving right to left, shown in Figure C.2(a)), where the end configuration matches the start configuration. Because the solutions to the differential equations are unique, and given the spatial symmetry of the parameters in our model, the trajectory shown in C.2(b) must also be a solution to the differential equations. Another way to see see that this must be a solution, is that it is simply the same solution shown in (a) but observed from the other side of the 2-D plane. If we again take the motion shown in (a) and reverse time, the trajectory for that system would look like Fig. C.2(c) due to the time reversibility of the differential equations (*a solution where time has been reversed is also a solution to this set of differential equations*). Note though that both of the systems pictured in Fig.C.2(b) and C.2(c) have the same initial conditions. Again, since the solutions for initial value problems of well-behaved (continuous and first-derivative continuous) ordinary differential equations are unique that means that the two trajectories shown in Fig.s C.2(b) & (c) must be the same trajectory. The only way that they can be the same trajectory is for the that trajectory to be mirror reflection symmetric about a vertical line passing through the support-hand.

Another way to see the above argument is to look at the equations of motion for the two-link system, eqn.(C.1)&(C.2), and make the following substitutions: $\theta_1 = -\theta_1$ and $\theta_2 = -\theta_2$. The equations of motion both before and after the substitution are identical.

$$\begin{aligned}
\theta_1'' = &-(P^2\sin(2\theta_2-\theta_1) + P^2\theta_1'^2\sin(2\theta_2-2\theta_1)+\\
&(2P^3+2R^2P)\theta_2'^2\sin(\theta_2-\theta 1)+\\
&(2P^3-3P^2+2PR^2-4R^2)\sin(\theta_1))/\\
&(P^2\cos(2\theta_2-2\theta_1)-2R^4+\\
&(-4P^2+4P-4)R^2-2P^4+4P^3-3P^2)
\end{aligned} \tag{C.1}$$

$$\theta_2'' = (P^2\theta_2'^2\sin(2\theta_2 - 2\theta_1) + (2P^3 - 4P^2 + 4P + 2R^2P)\theta_1'^2\sin(\theta_2 - \theta_1) + (2P - P^2)\sin(\theta_2 - 2\theta_1) + (2P^3 + 3P^2 + 2P + 2R^2P)\sin(\theta_2))/ (P^2\cos(2\theta_2 - 2\theta_1) - 2R^4 + (-4P^2 + 4P - 4)R^2 - 2P^4 + 4P^3 - 3P^2) \quad \text{(C.2)}$$

The above equations have been non-dimensionalized with prime($'$) denoting derivatives with respect to the non-dimensionalized time, τ. The non-dimensional variables are given in the following table:

non-dimensional center of mass location	$P = p/l$
non-dimensional radius of gyration	$R = \sqrt{I_{cm}/ml^2}$
non-dimensional time	$\tau = t/\sqrt{l/g}$

The solutions for the motions that are of interest must be symmetric about one or the other of these four configurations (see Fig. C.1): ($\theta_1 = 0$,$\theta_2 = 0$), ($\theta_1 = 0$,$\theta_2 = \pi$), ($\theta_1 = \pi$,$\theta_2 = 0$), ($\theta_1 = \pi$,$\theta_2 = \pi$). In other words, the motion of interest must be symmetric about a vertical line going through the "pivot hand," which was the same conclusion that was reached with the above argument. Note that this is the only model for which we proved that solutions must be symmetric.

C.3 Remarks on the two-link model results

Many collisionless motions were found for the two-link model since a brute force method was used Gomes (2005). The collisionless motions found tend to be divided into two distinct groups. One group consists of the motions in which the system starts and finishes the motion with the "swing hand" at the same location as the "pivot hand." These motions have no net forward displacement. The other, more interesting, group consists of motions in which the "swing hand" starts and finishes the motion at two distinct points a non-zero distance apart, allowing the system to move forward by letting go of the ceiling with the "pivot hand" and grabbing on with the "swing hand." One possible explanation for why the motions found tend to divide so well into these two groups comes from the division of the possible initial configurations into two groups. Since both "hands" must be touching the ceiling, for a given initial potential energy there are only two configurations which will satisfy this requirement ($\theta_1 = \pi - \theta_2$, $\theta_1 = \theta_2 + \pi$). Fig. C.3 shows that for a given energy level one of the possible configurations has both "hands" in the same location and the other does not. So for every energy level there are two groups

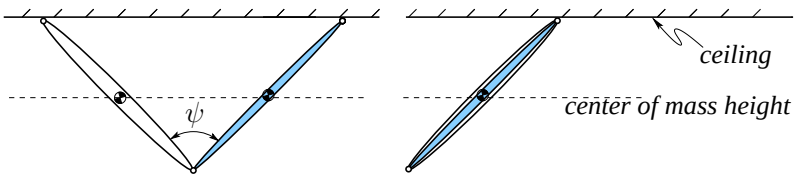

Fig. C.3. Possible initial configurations

of initial conditions, one where the two links overlap and the other where the two links are separated by some angle.

Another way to see why we get two sets of solutions would be to form our map equation to start with both hands on the ceiling and take our Poincare map section to be the point where $\theta_1 = 0$. Then we would see that our initial conditions could be broken up into two one-parameter families. One set would be parameterized by the non-zero relative angle between the two links(ϕ) where ($0 < \phi < 2\pi$). The other set would have a zero relative angle between the two links, and be parametrized by the angle between the links and gravity ($0 < \theta_1 < 2\pi$).